Adsorption of Surfactant Lipids by Single-Walled Carbon Nanotubes in Mouse Lung upon Pharyngeal Aspiration

Alexander A. Kapralov,[†,‡] Wei Hong Feng,[†,‡] Andrew A. Amoscato,[†,‡] Naveena Yanamala,[†,‡] Krishnakumar Balasubramanian,[†,‡] Daniel E. Winnica,[†,‡] Elena R. Kisin,[§] Gregg P. Kotchey,[⊥] Pingping Gou,[⊥] Louis J. Sparvero,[†,‡] Prabir Ray,[∥] Rama K. Mallampalli,[∥] Judith Klein-Seetharaman,[¶] Bengt Fadeel,[#] Alexander Star,[⊥] Anna A. Shvedova,[§] and Valerian E. Kagan[†,‡,*]

[†]Center for Free Radical and Antioxidant Health and [‡]Department of Environmental and Occupational Health, University of Pittsburgh, Pittsburgh, Pennsylvania 15260, United States, [§]Pathology and Physiology Research Branch, Health Effects Lab Division, National Institute for Occupational Safety and Health, Morgantown, West Virginia 26505, United Stages, [⊥]Department of Chemistry, [∥]Department of Medicine, Division of Pulmonary, Allergy and Critical Care Medicine, and [¶]Department of Structural Biology, University of Pittsburgh, Pittsburgh, Pennsylvania 15260, United States, and [#]Division of Molecular Toxicology, Institute of Environmental Medicine, Karolinska Institutet, Stockholm, Sweden

ABSTRACT The pulmonary route represents one of the most important portals of entry for nanoparticles into the body. However, the *in vivo* interactions of nanoparticles with biomolecules of the lung have not been sufficiently studied. Here, using an established mouse model of pharyngeal aspiration of single-walled carbon nanotubes (SWCNTs), we recovered SWCNTs from the bronchoalveolar lavage fluid (BALf), purified them from possible contamination with lung cells, and examined the composition of phospholipids adsorbed on SWCNTs by liquid chromatography mass spectrometry (LC-MS) analysis. We found that SWCNTs selectively adsorbed two types of the most abundant surfactant phospholipids: phosphatidylcholines (PC) and phosphatidylglycerols (PG). Molecular speciation of these phospholipids was also consistent with pulmonary surfactant. Quantitation of adsorbed lipids by LC-MS along with the structural assessments of phospholipid binding by atomic force microscopy and molecular modeling indicated that the phospholipids (~108 molecules per SWCNT) formed an uninterrupted "coating" whereby the hydrophobic alkyl chains of the phospholipids were adsorbed onto the SWCNT with the polar head groups pointed away from the SWCNT into the aqueous phase. In addition, the presence of surfactant proteins A, B, and D on SWCNTs was determined by LC-MS. Finally, we demonstrated that the presence of this surfactant coating markedly enhanced the *in vitro* uptake of SWCNTs by macrophages. Taken together, this is the first demonstration of the *in vivo* adsorption of the surfactant lipids and proteins on SWCNTs in a physiologically relevant animal model.

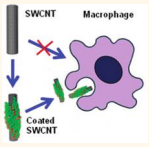

KEYWORDS: carbon nanotubes · surfactant · macrophages

The numerous emerging applications of nanotechnologies necessitate a detailed understanding of the interfaces of nanomaterials with biological systems, including interactions with components of biofluids, especially at sites of entry of nanomaterials into the body. The lung is one of the main portals of entry for inhaled nanoparticles where they can interact with pulmonary biosurfaces such as cells and surfactant.[1] Subsequently, the inhaled nanoparticles may translocate from the lung into secondary target organs in a size- and surface-charge-dependent manner.[2]

Pulmonary surfactant consists of lipids (90%) and proteins (10%) and plays a crucial role in respiratory functions as a biophysical entity to reduce surface tension at the air–water interface. It facilitates gas exchange and alveolar stability and acts as an innate component of the lung's immune system to maintain sterility and balance immune reactions in the distal airways. Surfactant proteins (SP-A, SP-B, SP-C, and SP-D) and their distinct interactions with surfactant phospholipids are essential for the ultrastructural organization, stability, metabolism, and the lowering of surface tension to prevent alveolar collapse. In addition, SP-A and SP-D bind pathogens, inflict damage to microbial membranes, and regulate microbial phagocytosis and activate or deactivate inflammatory responses by alveolar macrophages.[3,4] Previous *in vitro* studies have demonstrated the adsorption of pulmonary surfactant phospholipids on nanosized gold particles and carbon black particles.[5]

Upon incubation with human plasma, nanoparticles have been shown to acquire a "corona" of proteins as well as lipids[6–8] that may influence cellular uptake and toxicity of nanomaterials.[9,10] For instance, Ge *et al.*[11] reported that the binding of human serum proteins to single-walled carbon nanotubes (SWCNTs) strongly reduced their toxic potential. We previously showed that

* Address correspondence to kagan@pitt.edu.

Received for review February 10, 2012 and accepted March 31, 2012.

Published online April 01, 2012
10.1021/nn300626q

the adsorption of an anionic phospholipid, phosphatidylserine (PS), onto the surface of SWCNTs promoted their uptake by murine and human macrophages and dendritic cells of the immune system.[12] However, the *in vivo* adsorption of biomolecules on nanomaterials following pulmonary exposure has not been characterized. The binding of components of pulmonary surfactant with the surface of nanoparticles may be compared with the opsonization of pathogens, for example, bacteria, viruses, or allergen particles.[13] Thus, it is likely that the coating of nanoparticles with proteins and/or lipids will confer a new biological "identity" defining, to a large extent, their recognition by cells of the innate immune system which, in turn, may affect their biodistribution.[14]

In the present study, we determined the interactions of SWCNTs with pulmonary surfactant components and the consequences of surfactant coating for their phagocytosis by macrophages. Using an established mouse model of pharyngeal aspiration of SWCNTs, we recovered SWCNTs with the bronchoalveolar lavage fluid (BALf) after aspiration, purified them from possible contamination by lung alveolar cells, and examined their phospholipid composition by LC-MS analysis. We found that SWCNTs specifically adsorbed major surfactant phospholipids along with surfactant proteins A, B, and D. This surfactant-like "aura" of SWCNTs markedly enhanced their recognition and uptake by RAW264.7 macrophages.

RESULTS AND DISCUSSION

***In Vivo* Coating of SWCNTs by Lipid and Protein Components of Surfactant.** To characterize the ability of SWCNTs to adsorb pulmonary lipids *in vivo*, LC-MS analysis of phospholipids in organic extracts of SWCNTs recovered by sucrose gradient purification from BALf of mice 2 and 24 h after pharyngeal aspiration of SWCNTs was performed (Figure 1A–C). The presence of cells in BALf was excluded prior to MS analysis (see Materials and Methods). The composition of the SWCNT-adsorbed phospholipids was essentially the same at the 2 and 24 h time points. Although all major classes of phospholipids were detected, the spectra of nanomaterial-bound lipids reflected lipid profiles typical of surfactant lipids. Two phospholipids of BALf, PC and PG,[15–18] were the dominant components in the spectra (Figure 1A). No phospholipid signals were detected in the spectra of extracts from control samples obtained from non-exposed animals (Figure 1B). Similarly, control extracts of the SWCNT suspensions were devoid of lipid signals (Figure 1C). Expectedly, relatively low intensity signals from PC species were observed in the negative ion mode LC-MS chromatograms (Figure 1A). MALDI-MS analysis of the SWCNT lipids in positive ionization mode confirmed the predominance of PC whereby DPPC (16:0/16:0) represented the dominant PC species

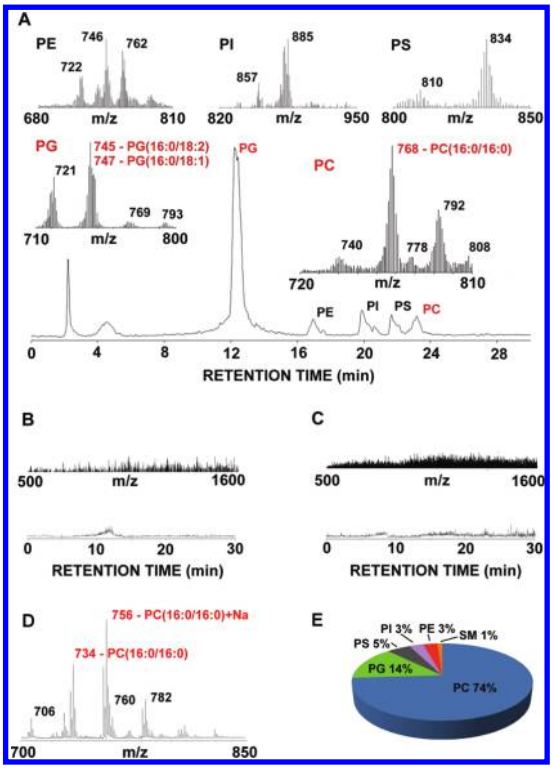

Figure 1. MS analysis of lipids adsorbed on SWCNTs 24 h after pharyngeal aspiration in mice. (A) Base peak chromatogram and LC/MS spectra of individual lipid classes (insets) of material extracted from SWCNTs from mice after pharyngeal aspiration. PC dominates with respect to amount, although this is not reflected in the TIC trace since PC ionizes to a much lesser extent in negative ion mode. (B) Control spectrum (top panel) and chromatogram (bottom panel) from BAL fluid run over sucrose gradient. (C) Control spectrum (top panel) and chromatogram (bottom panel) from nontreated CNTs. Note that typical lipid mass ions were not seen in the absence of SWCNTs, indicating the absence of cell contamination from extracts of SWCNT suspensions alone. (D) Positive mode MALDI spectrum of lipids extracted from SWCNTs from mice after pharyngeal aspiration confirming PC (16:0/16:0, *m/z* 734, sodium adduct, *m/z* 756) as one of the major lipid species. (E) Distribution of phospholipid classes in material associated with SWCNTs. Only one species of sphingomyelin was present which was in very low abundance. Fatty acyl chain distributions as well as percent abundances are given in Table 1 and indicate that dipalmitoyl phosphatidylcholine (DPPC, *m/z* 768, chloride adduct) dominates (up to 60%) as the major PC species while 16:0/18:1, 16:0/18:2 PG (combined), and 16:0/16:0 PG dominate as the major PG species (up to 52 and 26%, respectively). The most abundant species of PC and PG are highlighted in red.

(Figure 1D). LC-MS analysis revealed five individual molecular species of PC (*m/z* 740, 768, 778, 792, and 808, which run as Cl adducts) and four species of PG (*m/z* 721, 747, 769, and 793) (Figure 1A). Quantitative analysis performed by LC-MS indicated that PC was accountable for 74% of the total phospholipids adsorbed on the SWCNT (178.0 pmol/nmol of inorganic lipid phosphorus (Pi) (Figure 1E). PG represented 14% of the SWCNT phospholipids (31.3 pmol/nmol of Pi). The remaining 12% of lipids was distributed fairly equally among PS, PI, and PE (5, 3, and 3%, respectively)

TABLE 1. Fatty Acyl Chain Analysis of the Dominant PC and PG Species

m/z	fatty acyl chains	% abundance
	phosphatidylglycerol	
745, 747	16:0/18:2, 16:0/18:1	52.0
721	16:0/16:0	25.6
793	18:2/20:4	13.1
769	18:2/18:2	9.3
	phosphatidylcholine[a]	
768	16:0/16:0	58.8
792	16:1/18:1, 16:0/18:2	19.1
740	16:0/14:0	11.2
778	16:0p/18:2, 16:1p/18:1	5.7
808	18:0p/18:1, 18:0/20:4 (no adducts)	5.2
	phosphatidylethanolamine	
746	18:0/18:0	44
762	18:2/20:4, 16:0/22:6	36
722	16:0p/20:4	20
	phosphatidylinositol	
885	18:0/20:4	77
857	16:0/20:4	23
	phosphatidylserine	
834	18:0/22:6	80
810	18:0/20:4	20
	sphingomyelin[a,b]	
767	d18:0/18:0	100

[a] Masses ran as Cl adducts, except where indicated. [b] sphingoid base/acyl chains, *p*-plasmenyl.

with minimal amounts (1%) of sphingomyelin. Specifically, three species of PE (*m/z* 722, 746, and 762), two species each for PI (*m/z* 885 and 857) and PS (*m/z* 810 and 834), and only one species of sphingomyelin were detected. Fatty acyl composition and percent abundances corresponding to these species of phospholipids are given in Table 1. Dipalmitoyl phosphatidylcholine (DPPC, *m/z* 768, chloride adduct) dominated (up to 60%) as the major PC species while 16:0/18:1 PG, 16:0/18:2 PG (combined), and 16:0/16:0 PG represented the major PG species (up to 52 and 26%, respectively). These assessments are in excellent agreement with the published estimates of the phospholipid content (~90% of total lipids) in BALf.[15−18] The ranges for major phospholipid components of the surfactant have been reported as follows: PC, 70−80% (up to 70% of this can be DPPC); PG, 7−18%; PS, 3−5%; PI, 2−4%; PE, 2−3%; and SM, < 2%. Notably, this surfactant-specific pattern of SWCNT-adsorbed phospholipids and their individual molecular species is distinctly different from the phospholipid profile of the mouse lung where PC, PE, and PS represent the most abundant species.[19] Furthermore, the molecular speciation of the SWCNT-adsorbed lipids detected here is also markedly different from lung phospholipids. Indeed, PC (16:1/18:2) and PC (16:0/20:4) are the most abundant pulmonary species of phospholipids in the lung.[19]

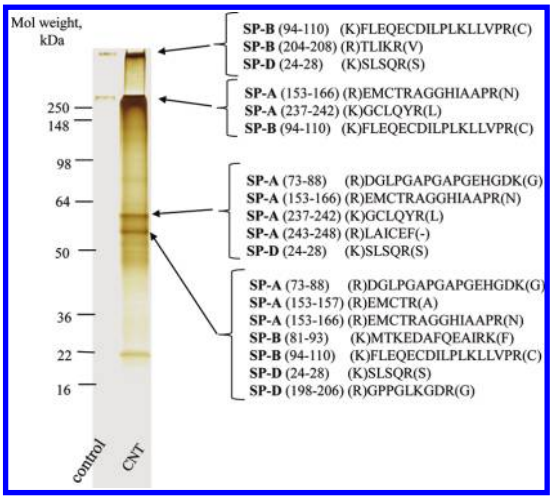

Figure 2. Identification of proteins bound to SWCNTs 24 h after pharyngeal aspiration in mice. SDS-PAGE of BALf proteins associated with SWCNTs. The gels were stained by SilverSNAP stain kit. MS analysis of SWCNT-bound proteins recovered from in-gel digestion revealed the presence of several surfactant proteins (SP). The sequences determined from matches of mass ions by mass profile fingerprinting are shown.

Given that SWCNTs selectively adsorbed surfactant phospholipids following pharyngeal aspiration, we further conducted protein analysis to determine the extent to which surfactant proteins were also bound to SWCNTs. Proteomic analysis of SWCNT-associated proteins by SDS-PAGE with subsequent MS of in-gel digests revealed several bands represented mostly by proteins with molecular weights of more than 50 kDa; some of the proteins had very high molecular weights and could not penetrate into stacking or running gel (Figure 2). Similar to the data with phospholipids, the composition of the SWCNT-adsorbed proteins was essentially the same at the 2 and 24 h time points. MS analysis of SWCNT-bound proteins was performed to identify the possible presence of surfactant proteins. Four protein bands were selected based on their intensity by silver staining and their ability to be excised as a single protein band for analysis. Approximately 80 peaks were detected in the LC-MS spectra of the tryptic digests from each gel band. Few, if any, of these were strong enough for MS/MS identification. This was somewhat expected from the limited amount of proteins associated with SWCNTs and their recovery from in-gel digestion. Nonetheless, three mouse lung-related proteins (surfactant-associated proteins A, B, and D, Figure 2) were matched by mass profile fingerprinting. Three to seven mass profile fragments of surfactant A, B, and D proteins in various combinations were detected in the four gel bands. SP-A, SP-B, and SP-D have all been detected in mouse BALf.[20−22] Since the samples were not reduced prior to the SDS-PAGE separation, these proteins presumably aggregated and appeared as oligomers in several of the gel bands (Figure 2). Taken together, our data show that surfactant

lipids and proteins are adsorbed on the SWCNT surface after pharyngeal aspiration in mice.

Two families of surfactant-associated proteins have been purified from surfactant: the high molecular weight hydrophilic SP-A and SP-D and the low molecular weight hydrophobic SP-B and SP-C.[4] We found that SP-A, SP-B, and SP-D, but not SP-C, were adsorbed on the SWCNT. One of the possible reasons for this is the relatively lower abundance of SP-C. Indeed, SP-A constitutes approximately 3−4% of the total mass of isolated surfactant and 50% of the total surfactant protein, while SP-B comprises 10% (w/w) of the total surfactant protein. Surfactant proteins SP-C and SP-D were found in smaller amounts.[4] Our previous work established that SWCNTs induce robust inflammation in the lung of mice[23] accompanied by the production and release of a variety of inflammatory mediators, including TNF-α. SP-C expression can be regulated by inflammation (*e.g.*, following bleomycin treatment, hyperoxia, or by pathogens), mostly due to the released cytokines, particularly TNF-α, which has been shown to decrease SP-C transcription and protein expression levels.[24,25] Thus, SP-C levels are expectedly lower in a pro-inflammatory environment induced by the SWCNT exposure. Another reason of the absence of SP-C in our gels is its characteristic very small molecular weight (of approximately 3.7 kDa) and high degree of hydrophobicity. In addition, SP-C is soluble in 80% acetonitrile or chloroform, and palmitoylation of its cysteine residues adds to the hydrophobic character of this protein.[26,27] Our computer modeling indicated that the fatty acyl chains of phospholipids preferentially associate with SWCNTs with the polar (hydrophilic) head groups oriented outward toward the solution. This may diminish the interactions between the low concentrations of the very hydrophobic SP-C molecules with SWCNTs coated with high amounts of surfactant phospholipids.

We attempted to assess what fraction of lipids and proteins present in surfactant was adsorbed by SWCNTs. In these evaluations, we kept in mind the likely possibility that SWCNTs have been taken up by cells and/or redistributed from the airways to other compartments of the lung. These SWNTs will not be recovered in BALf, hence their adsorbed constituents will remain undetected. Our calculation of the total amount of phospholipids retrieved from extracts of the coated SWCNT was in the range of 20−30 μg per animal. Assuming that the total amount of phospholipids in the surfactant of rodent species is approximately 220 μg per animal,[28] the phospholipids recovered from the SWCNT represented approximately 9−14% of the total amount of lipid found in surfactant. Further, lipids account for more than 80% of whole isolated surfactant by weight, while proteins make up ∼10%. About 50−80% of this amount is plasma proteins, and the remainder is made up of the surfactant-specific proteins.[29,30] Thus the total amount of proteins in the surfactant can be estimated as approximately 20 μg. The amount of proteins adsorbed on SWCNTs under our conditions was approximately 10−15 μg/5 animals (2−3 μg/animal). This leads to ∼10−15% of surfactant proteins adsorbed on SWCNTs. This suggests that lipids and proteins were adsorbed on SWCNTs in approximately the same ratio as that found in surfactant. Similar conclusions can be made from our results that different species of lipids adsorbed on SWCNTs a ratio similar to that found in surfactant.

Structural Characterization of Interactions of Surfactant Lipids and Proteins with SWCNTs. To assess the structural aspects of interactions of surfactant lipids and proteins with SWCNTs, we employed atomic force microscopy (AFM). This technique was applied on "naked" SWCNTs, SWCNTs incubated with either phospholipids or surfactant protein D (SP-D), and SWCNTs incubated with both phospholipids and SP-D. AFM revealed that the naked SWCNT lengths varied from 100 to 400 nm with a mean diameter of 1.7 ± 0.5 nm (n = 50, Figure 3A,B). SWCNTs incubated with the surfactant phospholipids appeared to be homogeneously coated with phospholipids, yielding a mean diameter of 4.9 ± 2.3 nm (n = 50, Figure 3C,D) and a mean lipid layer of 3.2 ± 1.8 nm. SP-D produced a continuous coating on SWCNTs with an wrapping-like pattern, which bestowed a mean height of 4.6 ± 1.9 nm (n = 50) and mean protein layer of 2.9 ± 1.4 nm onto the SWCNT (Figure 3E,F). Finally, SWCNTs incubated with both phospholipids and SP-D exhibited an uninterrupted coating pattern with an average height profile of 7.9 ± 3.8 nm (n = 50, Figure 3G,H). As a result, the mean height of the combined phospholipid and SP-D layer demonstrated a thickness of 6.2 ± 3.3 nm, which is consistent with the data described above.

Molecular Modeling of the Surfactant Coating. Molecular modeling was used to further refine our understanding of SWCNT interactions with surfactant phospholipids and proteins. The lipid species of the pulmonary surfactant, DPPC (16:0/16:0), PG (16:0/18:2), PS (18:0/22:6), and PE (18:0/18:0), were docked to SWCNTs using Autodock Vina.[31] The predicted binding mode of DPPC, PG, PS, and PE on SWCNTs is shown in Figure 4. In all cases, the analysis of the binding of the two major phospholipid species, PG and DPPC, indicated that the hydrophobic alkyl chains of these phospholipids were adsorbed onto the SWCNT with their polar head groups pointed away from the SWCNT into the aqueous phase. In particular, a tilt in the orientation of the lipid hydrophobic chain was observed with respect to the alignment of the lipids on the SWCNT (Figure 4A, C−E). A total of eight conformations out of nine were observed to align in this way, except for one case where the hydrophobic chain was found to be aligned parallel to the SWCNT axis (Figure 4B). The alignment of lipid on the SWCNTs and tilt in its orientation was

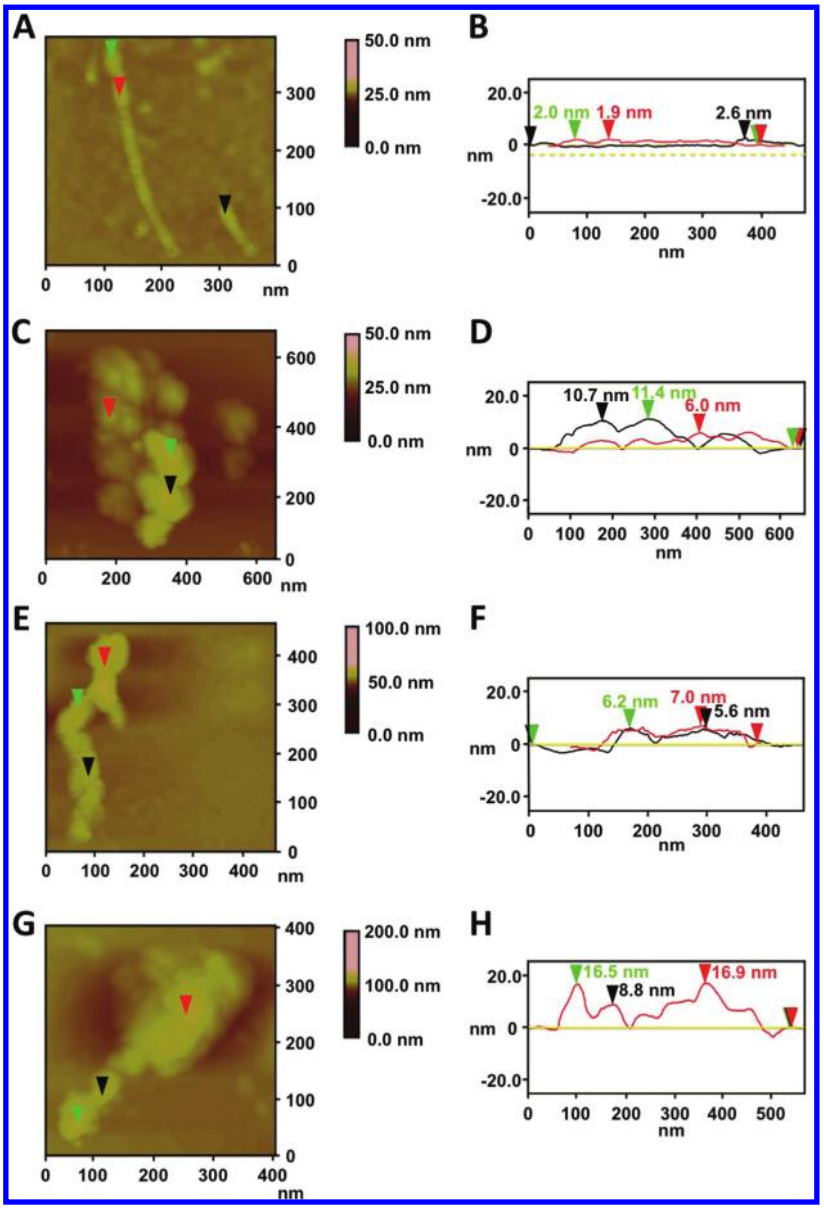

Figure 3. Structural characterization of interactions of surfactant lipids and proteins with SWCNTs by AFM. (A) AFM height image and (B) section analysis of carboxylated SWCNTs with a height profile of 1.9 nm (red arrow), 2.0 nm (green arrow), and 2.6 nm (black arrow). (C) AFM height image and (D) section analysis of lipid-coated carboxylated SWCNTs. The lipid-coated carboxylated SWCNTs demonstrated a height profile of 6.0 nm (red arrow), 11.4 nm (green arrow), and 10.7 nm (black arrow). (E) AFM height image and (F) section analysis of SP-D-coated carboxylated SWCNTs; the height profile for the SP-D-coated carboxylated SWCNT was determined to be 7.0 nm (red arrow), 6.2 nm (green arrow), and 5.6 nm (black arrow). (G) AFM height image of phospholipid/SP-D-coated carboxylated SWCNTs. (H) Section analysis indicated that the phospholipid/SP-D-coated SWCNT height profile was 16.9 nm (red arrow), 16.5 nm (green arrow), and 8.8 nm (black arrow).

attributed to hydrogen bonding between the SWCNT and the hydrophobic lipid chain.[32] Using the lowest energy tilted conformation of PG, we further generated a model by shifting the predicted conformation along the SWCNT axis to understand the progressive lipid coating on the SWCNT (Figure 4F). The model is in full agreement with the regular pattern of striations observed in the AFM studies (Figure 3) and is similar to the cylindrical encapsulation model described previously for detergents.[33] This type of coating may lead to complete masking and protection of the hydrophobic surface of the SWCNT from the aqueous environment. On the basis of these assessments of phospholipid topography on SWCNTs, we calculated the number of phospholipid molecules adsorbed on a single SWCNT. A contact area of ~20 nm per lipid molecule was estimated between the lipid hydrophobic chain and the SWCNT from the docking studies (Figure 4). Assuming a SWCNT of length 400 nm with a diameter of 1.7 nm and a total surface area of ~2141.7 nm^2 ($2\pi r^2 + 2\pi rh$), the total number of phospholipids required to coat the SWCNT would be ~108/SWCNT. This evaluation is in excellent agreement with independent calculations based on LC-MS measurements of phospholipids

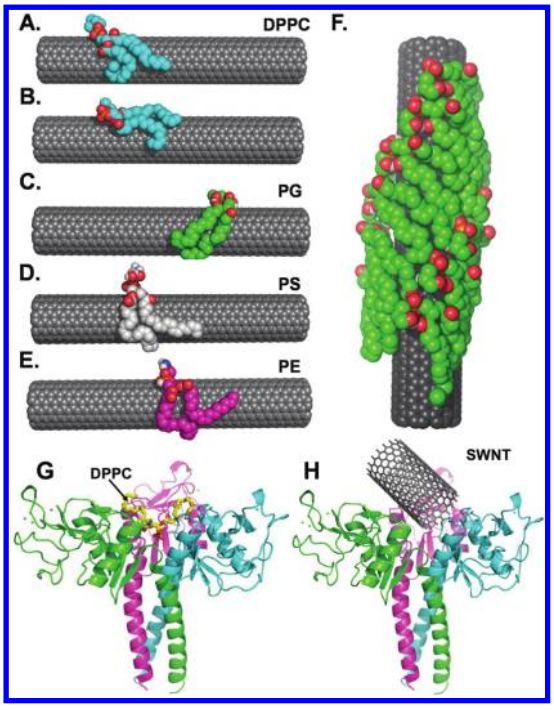

Figure 4. Computer modeling of SWCNTs binding with phospholipids and SP-D. The predicted binding pose of (A) lowest energy conformation of DPPC, (B) DPPC bound along the axis of SWCNT, lowest energy conformation of (C) PG, (D) PS, and (E) PE. (F) Lipid coating model generated using the PG-bound form of SWCNT shown in (C). The SWCNT is represented as spheres and colored in gray. The different phospholipids DPPC, PG, PS, and PE are rendered as spheres and colored in cyan, green, white, and magenta, respectively. In all cases, the N, O, and P atoms are colored in blue, red, and orange, respectively. The predicted binding sites of DPPC (G) and SWCNTs (H) on SP-D. The 3D structure of SP-D is colored according to the different chains and is represented as a cartoon. The structures of both DPPC and SWCNT are represented as sticks. The SWCNT is colored in gray, and the structure of DPPC is colored based on its atoms; *i.e.*, carbon, oxygen, and nitrogen atoms in yellow, red, and blue, respectively.

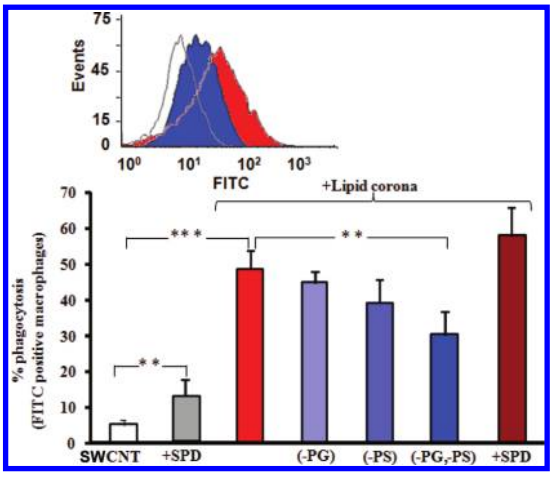

Figure 5. Effects of surfactant phospholipids and SP-D on the uptake of SWCNTs by RAW 264.7 macrophages. RAW264.7 macrophages were cultured overnight, then washed with PBS and incubated with SWCNTs or phospholipid-coated SWCNTs or phospholipid/SP-D-coated SWCNTs for 1 h at 37 °C. The cells were then washed, detached, and resuspended in 0.2% trypan blue for flow cytometric analysis. Phagocytosis is reported as the fraction of FITC-positive macrophages. Inset: histogram presentation of flow cytometry data for macrophages incubated with SWCNTs, alone (open trace), phospholipid-coated SWCNTs (red), phospholipid-coated SWCNTs deficient for PG and PS. The data are presented as percent phagocytosis mean values ± SD of three independent experiments; ** = $p < 0.01$, *** = $p < 0.001$.

according to which the number of phospholipid molecules in the coating was 115/SWCNT.

To obtain further insights into details of interactions of surfactant proteins with SWCNTs and surfactant phospholipids, we docked DPPC and SWCNTs to the available 3D crystal structure of SP-D (Figure 4G,H). Both lipids and SWCNTs were found to bind at a similar binding site involving the trimeric interface of the protein, indicating that SP-D can interact with both lipids and SWCNTs. The interaction of SP-D with DPPC was stabilized *via* the head group and not *via* the acyl chains. This indicates that SP-D has the potential to interact with SWCNTs precoated with surfactant phospholipids whereby the head groups are projected away from the SWCNTs. This is in agreement with our MS data documenting the presence of SP-D on SWCNTs. Unfortunately, we could not perform computer modeling assessments of SP-C with SWCNTs because the full-length 3D structure of SP-C is not available. The two available structures in Protein Data Bank (PDB) for SP-C correspond to the NMR-derived N-terminal propeptide (1−31) part and X-ray structure of BRICHOS domain (90−197, with sequence from 150 to 180 missing) of SP-C and lack the S-palmitoylation sites (*i.e.*, fatty acid chains), thus making it difficult to model the interaction of SP-C with SWCNT. It is likely that S-palmitoylation of SP-C *via* covalent attachment of fatty acids may lead to significant changes in its interaction with the polar head groups projected away from the plane of interaction.

The exposure of the polar head groups and the masking of the hydrophobic regions of the SWCNT could lead to enhanced recognition of SWCNTs by immune cells expressing specific receptors for lipid-dependent uptake of particulate matter or cellular debris. Indeed, the stereospecific binding of PS or PC exposed on the surface of apoptotic cells results in internalization of these cells by macrophages.[34,35]

Effects of Surfactant Lipids and SP-D on Phagocytosis of SWCNTs by Macrophages. To determine whether SWCNTs coated with surfactant phospholipids and/or surfactant proteins are recognized by macrophages, the internalization of SWCNTs with or without a surfactant coating was assessed using murine RAW264.7 macrophages as a model of phagocytic cells. Figure 5 demonstrates that the presence of adsorbed phospholipids significantly enhanced the uptake of SWCNTs when compared with uncoated SWCNTs. To determine if phagocytosis was dependent on the presentation of specific phospholipids on SWCNTs, the above

experiments were conducted using SWCNTs coated with combinations of adsorbed surfactant phospholipids whose composition was deficient for the lipid in question. As can be seen from Figure 5, the absence of PG, PS, and PG+PS reduced the number of macrophages with internalized targets by 4, 9, and 18%, respectively. To determine whether surfactant proteins could contribute to engulfment, uncoated SWCNTs or surfactant lipid SWCNTs were mixed with SP-D (1% w/w lipid) and incubated with macrophages as described above. Inclusion of SP-D alone increased the uptake of uncoated SWCNTs by ~7%, while its addition to SWCNTs with surfactant lipids enhanced the relative uptake by ~10% (Figure 5). Taken together, these data indicate that the association of SWCNTs with the lipid and protein components of the surfactant markedly altered the efficiency of their phagocytosis by macrophages.

These *in vitro* data suggest that the surfactant coating of SWCNTs may determine the recognition of these nanomaterials *in vivo* and therefore may impact the biodistribution and fate of these nanomaterials including their biodegradation.[36,37] The coating of nanoparticles has been described as a dynamic process whereby a significant exchange of noncovalently bound "hard" (long-lived) and "soft" coronas takes place; moreover, the corona is dynamic and may evolve as a result of the transfer of nanoparticles from one biological fluid (*e.g.*, plasma) into another (*e.g.*, cytosolic fluid).[38,39] Notably, a recent report indicates that the binding efficiency to cell lysate proteins appears to depend on the characteristics of the nanomaterial surface, whereas the adsorbed plasma proteins were suggested to be involved in particle phagocytosis and covered the nanomaterial independently of its surface properties.[40−42] Gasser *et al.*[5] provided evidence that the binding of plasma proteins to MWCNTs was altered when MWCNTs were previously coated with Curosurf, a natural surfactant preparation from pig. However, the present study provides the first evidence of the selective formation of a surfactant-derived lipid−protein coating on SWCNTs in an animal model of pulmonary exposure.

CONCLUSIONS

In summary, this work is the first demonstration of the *in vivo* adsorption of the surfactant lipids and proteins on SWCNTs in an animal model. Using LC-MS analysis, we found that SWCNTs recovered from the bronchoalveolar lavage fluid selectively adsorbed typical surfactant phospholipids phosphatidylcholine (PC) and phosphatidylglycerol (PG) and surfactant proteins A, B, and D. Molecular modeling indicates that the adsorbed phospholipids formed an uninterrupted "coating" whereby the hydrophobic alkyl chains of the phospholipids were adsorbed onto the SWCNT with the polar head groups pointed away from the SWCNT into the aqueous phase. The presence of the surfactant coating markedly enhanced the *in vitro* uptake of SWCNTs by macrophages. The present findings are essential for our understanding of the toxicological behavior of these nanomaterials but may also have important implications for nanomedicine and pulmonary delivery of drug-loaded nanoscale carriers.

MATERIALS AND METHODS

Reagents. DMEM cell culture medium, fetal bovine serum (FBS), and antibiotics were purchased from Invitrogen (Carlsbad, CA). 1,2-Dipalmitoyl-*sn*-glycero-3-phosphocholine (DPPC), 1,2-dioleoyl-*sn*-glycero-3-phospho-L-serine (DOPS), 1,2-dioleoyl-*sn*-glycero-3-phosphoglycerol (DOPG), 1,2-dioleoyl-*sn*-glycero-3-phosphoethanolamine (DOPE), L-α-phosphatidylinositol (Liver, Bovine), and sphingomyelin (SM) (Brain, Porcine) were purchased from Avanti Polar Lipids (Alabaster, AL).

Preparation and Characterization of SWCNTs. SWCNTs (CNI Inc., Houston, TX) produced by the high-pressure CO disproportionation process (HiPco) technique[43] employing CO in a continuous-flow gas phase as the carbon feedstock and $Fe(CO)_5$ as the iron-containing catalyst precursor and purified by acid treatment to remove metal contaminates[44] were used in the study. Chemical analysis of trace metal (iron) in SWCNTs was performed at the Chemical Exposure and Monitoring Branch (DART/NIOSH, Cincinnati, OH) using nitric acid dissolution and inductively coupled plasma atomic emission spectrometry (ICP-AES). Analysis revealed that SWCNTs comprised 0.23 wt % iron. SWCNTs were routinely tested for bacterial endotoxin (LPS) contamination using the end point chromogenic LAL method, as previously described.[45] The mean diameter and surface area of SWCNTs was 1−4 nm and 1040 m^2/g, respectively. Surface area was determined by Brunauer, Emmett, and Teller (BET) analysis, and diameter and length were measured by TEM. The chemical cutting of SWCNTs was performed as reported previously.[46] Obtained short SWCNTs were dispersed in 25 mM HEPES buffer (pH 7.4; containing 150 mM NaCl) by sonication. For purity assessment and characterization of SWCNTs, we used several standard analytical techniques. TEM was employed to determine the length distribution (Supporting Information Figure S2A). Raman spectroscopy was implemented to visualize the D and G bands (Supporting Information Figure S2B). Diffuse reflectance infrared Fourier transform spectroscopy (DRIFTS) was also performed (Supporting Information Figure S2C). Preparation of FITC-SWCNTs was performed as described in the Supporting Information.

Cells. RAW264.7 mouse macrophage cells obtained from American Tissue Culture Collections (ATCC) were maintained in DMEM culture medium supplemented with 10% heat-inactivated fetal bovine serum (FBS), 100 units/mL penicillin, and 100 μg/mL streptomycin.

Animals. Specific pathogen-free adult female C57BL/6 mice were supplied by Jackson Lab (Bar Harbor, ME) and weighed 20.0 ± 1.9 g at the time of experiment. Animals were housed one mouse per cage receiving HEPA-filtered air National Institute for Occupational Safety and Health (NIOSH) animal facilities accredited by Association for Assessment and Accreditation of Laboratory Animal Care. Animals were supplied with water and certified chow 5020 (Purina Mills, Richmond, IN) *ad libitum* and were acclimated in the animal facility under controlled temperature and humidity for one week prior to use. All experimental procedures were conducted in accordance with

the guidelines of the Institute of Laboratory Animal Resources (National Research Council) and the experimental protocol (#07-AS-M-010), approved by the National Institute for Occupational Safety and Health (NIOSH) Institutional Animal Care and Use Committee.

Pharyngeal Aspiration of SWCNTs. Mouse pharyngeal aspiration was used for particulate administration.[47] Briefly, after anesthetization with a mixture of ketamine and xylazine (62.5 and 2.5 mg/kg given subcutaneously in the abdominal area), the mouse was placed on a board in a near-vertical position. The animal's tongue was extended with lined forceps, and a suspension (~50 μL, 80 μg/mouse) of SWCNT prepared in $Ca^{2+}-Mg^{2+}$-free PBS (PBS) was placed posterior of the pharynx and the tongue which was held until the suspension was aspirated into the lungs. Control mice were administered sterile $Ca^{2+}+Mg^{2+}$-free PBS as a vehicle. The mice were allowed to revive unassisted after approximately 30−40 min. All mice in SWCNT and PBS groups survived this exposure procedure.

Obtaining BALf from Mice. BALf samples were obtained from mice 2 or 24 h postpharyngeal aspiration. Mice were sacrificed with an intraperitoneal injection of sodium pentobarbital (>100 mg/kg) and exsanguinated. The trachea was cannulated with a blunted 22 gauge needle, and BAL was performed using cold sterile PBS at a volume of 0.9 mL for first lavage (kept separate) and 1.0 mL for subsequent lavages. Approximately 5 mL of BALf per mouse was collected in sterile centrifuge tubes.

SWCNT Isolation and Purification from BALf. Purified samples of SWCNTs were obtained by centrifugation of BALf through 50% sucrose. The schema used to isolate SWCNT from BALf is presented in Supporting Information Figure S4. In brief, freshly pooled BALf samples (5 mice per group) were centrifuged at 700*g* for 10 min to pellet cells together with SWCNTs. Pellets were resuspended in 1 mL of PBS, loaded on top of 3 mL of 50% sucrose, and centrifuged at 700*g* for 12 min. Light microscopy demonstrated that, after this procedure, practically all cells were located at the interface of PBS−sucrose, while the pellet contained only SWCNTs. The pelleted SWCNTs were further resuspended in PBS and washed four times (60 000*g*, 1 h) with the same buffer. No typical lipid mass ions were found during MS analysis of the material extracted from pellets obtained after the centrifugation of BALf from control mice (no SWCNTs) through the 50% sucrose, confirming the complete removal of cells using this procedure.

MS Analysis of Lipids Adsorbed on SWCNTs. Lipids were extracted using the Folch procedure as described previously[48] and analyzed by normal phase chromatography using a Luna normal phase silica column (3 μm particle size (100 A), 150 × 2 mm, Phenomenex, Torrance, CA) with a flow rate of 0.2 mL/min. Lipids were eluted using a linear gradient using solvents consisting of chloroform/methanol/30% ammonium hydroxide (80:19.5:0.5, v/v/v, solvent A) and chloroform/methanol/water/30% ammonium hydroxide (60:34:5.5:0.5, v/v/v/v, solvent B) over 30 min. Lipids were detected and analyzed by mass spectrometry on a TSQ 7000 triple quadrupole mass spectrometer. Mass spectrometer conditions were as follows: spray voltage, 5.0 kV; capillary, 250 °C; sheath gas, 20 psi. Tuning was optimized for all classes of phospholipids across the scan range. PG (*m/z* 609) and PC (*m/z* 628) were utilized as internal standards (IS) in samples for quantitation. All LC-MS samples were run in the negative ion mode in duplicate which allowed for the remaining sample to be utilized for inorganic phosphorus analysis. Matrix-assisted laser desorption ionization mass spectrometry (MALDI-MS) and MS/MS was performed with a Bruker Ultraflex II TOF/TOF mass spectrometer (Bruker Daltonics, Billerica, MA). The matrix compound utilized was 2,5-dihydroxybenzoic acid (DHB) as 98+% grade from Sigma-Aldrich (St. Louis, MO). Reflector-positive or reflector-negative modes were used for MALDI-MS as appropriate, and MALDI-MS/MS was performed using positive mode with a 2 Da mass isolation window.

Analysis of Surfactant Proteins Adsorbed on SWCNTs. For analysis of proteins associated with SWCNTs, water and intermediate phases formed during lipid extraction were combined and proteins were precipitated by addition of 3 volumes of acetone overnight. Proteins were pelleted by centrifugation at 10 000*g* for 30 min, dissolved in 2% SDS, and separated by 10% SDS-PAGE in Tris-glycine buffer. The gels were stained using a SilverSNAP stain kit (Thermo Fisher Scientific, Rockford, IL). For mass analysis, gel destaining was achieved by a 10 min incubation in a solution containing 15 mM $K_3Fe(CN)_6$, 50 mM $Na_2S_2O_3$ followed by several water washes. Gel pieces were reduced in the presence of dithiothreitol (DTT) followed by alkylation with iodoacetamide. Gel pieces were then washed, dehydrated, and dried. The proteins were subjected to overnight in-gel digestion with trypsin (Promega Gold brand, 25 ng/μL in 25 mM ammonium bicarbonate buffer (pH 7.8)). Peptides were extracted with 5% formic acid, 50% acetonitrile, and evaporated to near dryness. Tryptic peptides were analyzed by LC-MS on an Agilent Eclipse XDB-C18 2.1 mm × 100 mm reverse phase column (0.2 mL/min flow rate; solvent A: water/0.1% formic acid; B: acetonitrile/0.1% formic acid; gradient of 2 to 20% B in 10 min, 20 to 40% B in 40 min, 40 to 70% B in 15 min, 70 to 100% B in 15 min, hold at 100% B for 10 min, return to 2% B in 20 min). Mass spectrometry analysis was performed in-line with the LC using a Micromass Premier Q-TOF (Waters, Milford, MA) equipped with an ESI source and running in V-positive mode. Mass profile fingerprinting was performed using the Protein Prospector software developed at the University of California, San Francisco (see P.R. Baker and K.R. Clauser, http://prospector.ucsf.edu).

Computer Modeling of Interactions of SWCNTs with Surfactant Lipids. The lipid species of the pulmonary surfactant, DPPC (16:0/16:0), PG (16:0/18:2), PS (18:0/22:6), and PE (18:0/18:0) were docked to SWCNT using Autodock Vina.[31] The structures of the phospholipids were extracted from the lipid maps, and a SWCNT of diameter 1.3 nm was generated using the Nanotube Modeler Software (http://www.jcrystal.com/products/wincnt/index.htm). AutoDockTools (ATD) package (http://autodock.scripps.edu/resources/adt) was further used for formatting and converting the pdb files to pdbqt format. The docking was performed using the center of the SWCNT as the grid center and a grid box of size 75 Å × 75 Å × 75 Å. The resulting binding poses were clustered together, and the conformation with the lowest predicted binding energy was considered for further analysis in each case.

Atomic Force Microscopy (AFM) of SWCNTs with Adsorbed Lipids and SP-D. As a consequence of the equilibrium established between the CNTs and components of the dispersion (*i.e.*, lipids), the effect of the "state of dispersion" is critical to the overall nanoparticle presentation. Current SWCNT characterization methods have certain limitations. Indeed, the dry (*i.e.*, AFM) or vacuum (*i.e.*, TEM) characterization methods inadequately provide insight into the dynamic nature of a nanoparticle in the dispersion. Moreover, while dynamic light scattering (DLS) is a suitable technique for ascertaining the diameter of particles with spherical shapes in dispersions, only hydrodynamic diameters can be obtained for SWCNTs utilizing this technique. We selected AFM in tapping mode to characterize the surfaces of both naked and coated CNTs to obtain a snapshot of the dynamic system at a given point in time. Sample preparation was made by spin-coating 10 μL of sample at 1400 rpm on a freshly cleaved mica substrate that was pretreated with approximately 20 μL of 0.1% (w/w) poly-L-lysine (aq) through spin-coating, and the sample was permitted to dry at ambient temperature for 60 min prior to imaging. For imaging, "supersharp" Si probes (tip radius <5 nm, uncoated, App Nano (Santa Clara, CA)) and a multimode scanning probe microscope Veeco (Plainview, NY) were utilized in tapping mode to obtain height, phase, and sectional analysis data.

Coating of SWCNTs with Surfactant Lipids and SP-D. Small unilamellar vesicles (SUV) composed of the same proportion of lipid species as those adsorbed on SWCNTs (Figure 1D) were prepared by sonication in HBS (HEPES buffered saline, pH 7.4). SUVs were mixed with FITC-SWCNTs (SWCNTs/lipid ratio 120 μg/360 nmol) in the presence or absence of SP-D followed by sonication (3 × 15 s, ice bath). Unbound lipids and protein were removed by washing three times with HBS (30 000*g*, 30 min).

Phagocytosis of SWCNTs by RAW264.7 Mouse Macrophage Cells. RAW264.7 murine macrophages were cultured overnight, then washed with PBS and incubated with uncoated or surfactant lipid/protein-coated SWCNTs for 1 h at 37 °C. Unbound/uninternalized SWCNTs were removed by washing with PBS, and

internalized particles were determined by flow cytometry (FACScan, Becton-Dickinson, Rutherford, NJ) in the presence of trypan blue to exclude fluorescence from macrophage-bound SWCNTs.

Statistics. The results are presented as mean ± SD values from three experiments, and statistical analyses were performed using Student's *t* test. The statistical significance of differences was set at $p < 0.05$.

Conflict of Interest: The authors declare no competing financial interest.

Acknowledgment. This work was supported by grants from National Institute for Occupational Safety and Health (NIOSH) OH008282, National Institutes of Health NIEHS R01ES019304, HL70755, HL094488, U19AI068021, ES021068-01, National Occupational Research Agenda NORA 0HELD015, 927000Y, 927Z1LU, Nanotechnology Research Center (NTRC) 927ZJHF, National Science Foundation (NSF) CAREER 0449117, seventh Framework Program of the European Commission (EC-FP7-NANOMMUNE-214281), and the Science Foundation of Ireland, Strategic Research Cluster (SRC) BioNanointeract and Centre for Research on Adaptive Nanostructures and Nanodevices (CRANN), Higher Education Authority (HEA) and Programme for Research in Third-Level Institutions (PRTLI), and the Swedish Research Council for Environment, Agricultural Sciences and Spatial Planning (FORMAS), Cancer Center Support Grant (CCSG) P30 CA047904, and Environmental Protection Agency (EPA) FP-91713801. The findings and conclusions in this report are those of the authors and do not necessarily represent the views of the National Institute for Occupational Safety and Health.

Supporting Information Available: Characterization of SWCNTs employed in the study, supporting information, and methods. This material is available free of charge *via* the Internet at http://pubs.acs.org.

REFERENCES AND NOTES

1. Schleh, C.; Rothen-Rutishauser, B.; Kreyling, W. G. The Influence of Pulmonary Surfactant on Nanoparticulate Drug Delivery Systems. *Eur. J. Pharm. Biopharm.* **2011**, *77*, 350–352.
2. Choi, H. S.; Ashitate, Y.; Lee, J. H.; Kim, S. H.; Matsui, A.; Insin, N.; Bawendi, M. G.; Semmler-Behnke, M.; Frangioni, J. V.; Tsuda, A. Rapid Translocation of Nanoparticles from the Lung Airspaces to the Body. *Nat. Biotechnol.* **2010**, *28*, 1300–1303.
3. Chroneos, Z. C.; Sever-Chroneos, Z.; Shepherd, V. L. Pulmonary Surfactant: An Immunological Perspective. *Cell. Physiol. Biochem.* **2009**, *25*, 13–26.
4. Hermans, C.; Bernard, A. Lung Epithelium-Specific Proteins: Characteristics and Potential Applications as Markers. *Am. J. Respir. Crit. Care Med.* **1999**, *159*, 646–678.
5. Gasser, M.; Rothen-Rutishauser, B.; Krug, H. F.; Gehr, P.; Nelle, M.; Yan, B.; Wick, P. The Adsorption of Biomolecules to Multi-Walled Carbon Nanotubes Is Influenced by Both Pulmonary Surfactant Lipids and Surface Chemistry. *J. Nanobiotechnol.* **2010**, 31.
6. Cedervall, T.; Lynch, I.; Lindman, S.; Berggard, T.; Thulin, E.; Nilsson, H.; Dawson, K. A.; Linse, S. Understanding the Nanoparticle−Protein Corona Using Methods To Quantify Exchange Rates and Affinities of Proteins for Nanoparticles. *Proc. Natl. Acad. Sci. U.S.A.* **2007**, *104*, 2050–2055.
7. Lundqvist, M.; Stigler, J.; Elia, G.; Lynch, I.; Cedervall, T.; Dawson, K. A. Nanoparticle Size and Surface Properties Determine the Protein Corona with Possible Implications for Biological Impacts. *Proc. Natl. Acad. Sci. U.S.A.* **2008**, *105*, 14265–14270.
8. Zhang, H.; Burnum, K. E.; Luna, M. L.; Petritis, B. O.; Kim, J. S.; Qian, W. J.; Moore, R. J.; Heredia-Langner, A.; Webb-Robertson, B. J.; Thrall, B. D.; *et al.* Quantitative Proteomics Analysis of Adsorbed Plasma Proteins Classifies Nanoparticles with Different Surface Properties and Size. *Proteomics* **2011**, *11*, 4569–4577.
9. Dutta, D.; Sundaram, S. K.; Teeguarden, J. G.; Riley, B. J.; Fifield, L. S.; Jacobs, J. M.; Addleman, S. R.; Kaysen, G. A.; Moudgil, B. M.; Weber, T. J. Adsorbed Proteins Influence the Biological Activity and Molecular Targeting of Nanomaterials. *Toxicol. Sci.* **2007**, *100*, 303–315.
10. Ehrenberg, M. S.; Friedman, A. E.; Finkelstein, J. N.; Oberdorster, G.; McGrath, J. L. The Influence of Protein Adsorption on Nanoparticle Association with Cultured Endothelial Cells. *Biomaterials* **2009**, *30*, 603–610.
11. Ge, C.; Du, J.; Zhao, L.; Wang, L.; Liu, Y.; Li, D.; Yang, Y.; Zhou, R.; Zhao, Y.; Chai, Z.; *et al.* Binding of Blood Proteins to Carbon Nanotubes Reduces Cytotoxicity. *Proc. Natl. Acad. Sci. U.S.A.* **2011**, *108*, 16968–16973.
12. Konduru, N. V.; Tyurina, Y. Y.; Feng, W.; Basova, L. V.; Belikova, N. A.; Bayir, H.; Clark, K.; Rubin, M.; Stolz, D.; Vallhov, H.; *et al.* Phosphatidylserine Targets Single-Walled Carbon Nanotubes to Professional Phagocytes *in Vitro* and *in Vivo*. *PLoS One* **2009**, *4*, e4398.
13. Dunkelberger, J. R.; Song, W. C. Complement and Its Role in Innate and Adaptive Immune Responses. *Cell Res.* **2010**, *20*, 34–50.
14. Hellstrand, E.; Lynch, I.; Andersson, A.; Drakenberg, T.; Dahlback, B.; Dawson, K. A.; Linse, S.; Cedervall, T. Complete High-Density Lipoproteins in Nanoparticle Corona. *FEBS J.* **2009**, *276*, 3372–3381.
15. Veldhuizen, R.; Nag, K.; Orgeig, S.; Possmayer, F. The Role of Lipids in Pulmonary Surfactant. *Biochim. Biophys. Acta* **1998**, *1408*, 90–108.
16. Guthmann, F.; Haupt, R.; Schlame, M.; Stevens, P. A.; Rustow, B. Alveolar Surfactant Subfractions Differ in Their Lipid Composition. *Int. J. Biochem. Cell Biol.* **1995**, *27*, 1021–1026.
17. Numata, M.; Chu, H. W.; Dakhama, A.; Voelker, D. R. Pulmonary Surfactant Phosphatidylglycerol Inhibits Respiratory Syncytial Virus-Induced Inflammation and Infection. *Proc. Natl. Acad. Sci. U.S.A.* **2010**, *107*, 320–325.
18. Hallman, M.; Gluck, L. Phosphatidylglycerol in Lung Surfactant. III. Possible Modifier of Surfactant Function. *J. Lipid Res.* **1976**, *17*, 257–262.
19. Tyurina, Y. Y.; Tyurin, V. A.; Kaynar, A. M.; Kapralova, V. I.; Wasserloos, K.; Li, J.; Mosher, M.; Wright, L.; Wipf, P.; Watkins, S.; Pitt, B. R.; *et al.* Oxidative Lipidomics of Hyperoxic Acute Lung Injury: Mass Spectrometric Characterization of Cardiolipin and Phosphatidylserine Peroxidation. *Am. J. Physiol.* **2010**, *299*, L73–L85.
20. Gharib, S. A.; Nguyen, E.; Altemeier, W. A.; Shaffer, S. A.; Doneanu, C. E.; Goodlett, D. R.; Schnapp, L. M. Of Mice and Men: Comparative Proteomics of Bronchoalveolar Fluid. *Eur. Respir. J.* **2010**, *35*, 1388–1395.
21. Guo, Y.; Ma, S. F.; Grigoryev, D.; Van Eyk, J.; Garcia, J. G. 1-DE MS and 2-D LC-MS Analysis of the Mouse Bronchoalveolar Lavage Proteome. *Proteomics* **2005**, *5*, 4608–4624.
22. Zhang, L.; Wang, M.; Kang, X.; Boontheung, P.; Li, N.; Nel, A. E.; Loo, J. A. Oxidative Stress and Asthma: Proteome Analysis of Chitinase-like Proteins and FIZZ1 in Lung Tissue and Bronchoalveolar Lavage Fluid. *J. Proteome Res.* **2009**, *8*, 1631–1638.
23. Shvedova, A. A.; Murray, A. R.; Johnson, V. J.; Gorelik, O.; Arepalli, S.; Hubbs, A. F.; Mercer, R. R.; Keohavong, P.; Sussman, N.; Jin, J.; *et al.* Inhalation *vs.* Aspiration of Single-Walled Carbon Nanotubes in C57BL/6 Mice: Inflammation, Fibrosis, Oxidative Stress and Mutagenesis. *Am. J. Physiol.* **2008**, *295*, L552–L565.
24. Mulugeta, S.; Meers, M. F. Surfactant Protein C; Its Unique Properties and Emerging Immunomodulatory Role in the Lung. *Microbes Infect.* **2006**, *8*, 2317–2323.
25. Park, W. Y.; Goodman, R. B.; Steinberg, K. P.; Ruzinski, J. T.; Radella, F.; Park, D. R.; Pugin, J.; Skerrett, S. J.; Hudson, L. D.; Martin, T. R. Cytokine Balance in the Lungs of Patients with Acute Respiratory Distress Syndrome. *Am. J. Respir. Crit. Care Med.* **2001**, *164*, 1896–1903.
26. Creuwels, L. A. J. M.; van Golde, L. M. G.; Haagsman, H. P. The Pulmonary Surfactant System: Biochemical and Clinical Aspects. *Lung* **1997**, *175*, 1–39.
27. Curstedt, T.; Johansson, J.; Persson, P.; Eklund, A.; Robertson, B.; Lowenadler, B.; Jornvall, H. Hydrophobic Surfactant-Associated Polypeptides: SP-C Is a Lipopeptide with Two Palmitoylated Cysteine Residues, Whereas SP-B Lacks

Covalently Linked Fatty Acyl Groups. *Proc. Natl. Acad. Sci. U.S.A.* **1990**, *87*, 2985–2989.
28. Coonrod, J. D.; Jarrells, M. C.; Yoneda, K. Effect of Rat Surfactant Lipids on Complement and Fc Receptors of Macrophages. *Infect. Immun.* **1986**, *54*, 371–378.
29. Hamm, H.; Fabel, H.; Bartsch, W. The Surfactant System of the Adult Lung: Physiology and Clinical Perspectives. *Clin. Invest.* **1992**, *70*, 637–657.
30. Schürch, S.; Bachofenb, H.; Possmayer, F. Pulmonary Surfactant: Surface Properties and Function of Alveolar and Airway Surfactant. *Pure Appl. Chem.* **1992**, *64*, 1745–1750.
31. Trott, O.; Olson, A. J. AutoDock Vina: Improving the Speed and Accuracy of Docking with a New Scoring Function, Efficient Optimization, and Multithreading. *J. Comput. Chem.* **2010**, *31*, 455–461.
32. Wang, H.; Michielssens, S.; Moors, S.; Ceulemans, A. Molecular Dynamics Study of Dipalmitoylphosphatidylcholine Lipid Layer Self-Assembly onto a Single-Walled Carbon Nanotube. *Nano Res.* **2009**, *2*, 945–954.
33. Wallace, E. J.; Sansom, M. S. Carbon Nanotube/Detergent Interactions *via* Coarse-Grained Molecular Dynamics. *Nano Lett.* **2007**, *7*, 1923–1928.
34. Greenberg, M. E.; Sun, M.; Zhang, R.; Febbraio, M.; Silverstein, R.; Hazen, S. L. Oxidized Phosphatidylserine-CD36 Interactions Play an Essential Role in Macrophage-Dependent Phagocytosis of Apoptotic Cells. *J. Exp. Med.* **2006**, *203*, 2613–2625.
35. Santiago, C.; Ballesteros, A.; Martinez-Munoz, L.; Mellado, M.; Kaplan, G. G.; Freeman, G. J.; Casasnovas, J. M. Structures of T Cell Immunoglobulin Mucin Protein 4 Show a Metal-Ion-Dependent Ligand Binding Site Where Phosphatidylserine Binds. *Immunity* **2007**, *27*, 941–951.
36. Kagan, V. E.; Konduru, N. V.; Feng, W.; Allen, B. L.; Conroy, J.; Volkov, Y.; Vlasova, I. I.; Belikova, N. A.; Yanamala, N.; Kapralov, A.; *et al.* Carbon Nanotubes Degraded by Neutrophil Myeloperoxidase Induce Less Pulmonary Inflammation. *Nat. Nanotechnol.* **2010**, *5*, 354–359.
37. Shvedova, A. A.; Kapralov, A. A.; Feng, W.; Kisin, E. R.; Murray, A.; Mercer, R.; St. Croix, C.; Lang, M.; Watkins, S.; Konduru, N.; *et al.* Impaired Clearance and Enhanced Pulmonary Inflammatory/Fibrotic Response to Carbon Nanotubes in Myeloperoxidase-Deficient Mice. *PLoS One* **2012**, 10.1371/journal.pone.0030923.
38. Walczyk, D.; Bombelli, F. B.; Monopoli, M. P.; Lynch, I.; Dawson, K. A. What the Cell "Sees" in Bionanoscience. *J. Am. Chem. Soc.* **2010**, *132*, 5761–5768.
39. Lundqvist, M.; Stigler, J.; Cedervall, T.; Berggard, T.; Flanagan, M. B.; Lynch, I.; Elia, G.; Dawson, K. The Evolution of the Protein Corona around Nanoparticles: A Test Study. *ACS Nano* **2011**, *5*, 7503–7509.
40. Monopoli, M. P.; Walczyk, D.; Campbell, A.; Elia, G.; Lynch, I.; Bombelli, F. B.; Dawson, K. A. Physical-Chemical Aspects of Protein Corona: Relevance to *In Vitro* and *In Vivo* Biological Impacts of Nanoparticles. *J. Am. Chem. Soc.* **2011**, *133*, 2525–2534.
41. Sund, J.; Alenius, H.; Vippola, M.; Savolainen, K.; Puustinen, A. Proteomic Characterization of Engineered Nanomaterial–Protein Interactions in Relation to Surface Reactivity. *ACS Nano* **2011**, *5*, 4300–4309.
42. Simberg, D.; Park, J. H.; Karmali, P. P.; Zhang, W. M.; Merkulov, S.; McCrae, K.; Bhatia, S. N.; Sailor, M.; Ruoslahti, E. Differential Proteomics Analysis of the Surface Heterogeneity of Dextran Iron Oxide Nanoparticles and the Implications for Their *In Vivo* Clearance. *Biomaterials* **2009**, *30*, 3926–3933.
43. Scott, C. D.; Povitsky, A.; Dateo, C.; Gokcen, T.; Willis, P. A.; Smalley, R. E. Iron Catalyst Chemistry in Modeling a High-Pressure Carbon Monoxide Nanotube Reactor. *J. Nanosci. Nanotechnol.* **2003**, *3*, 63–73.
44. Gorelik, O. N.; Arepalli, S. Purification Procedures for Single-Wall Carbon Nanotubes. NASA contractor report, NASA/CR-2000-208926, **2000**.
45. Vallhov, H.; Qin, J.; Johansson, S. M.; Ahlborg, N.; Muhammed, M. A.; Scheynius, A.; Gabrielsson, S. The Importance of an Endotoxin-Free Environment during the Production of Nanoparticles Used in Medical Applications. *Nano Lett.* **2006**, *6*, 1682–1686.
46. Liu, J.; Rinzler, A. G.; Dai, H.; Hafner, J. H.; Bradley, R. K.; Boul, P. J.; Lu, A.; Iverson, T.; Shelimov, K.; Huffman, C. B.; *et al.* Fullerene Pipes. *Science* **1998**, *280*, 1253–1256.
47. Rao, G. V.; Tinkle, S.; Weissman, D. N.; Antonini, J. M.; Kashon, M. L.; Salmen, R.; Battelli, L. A.; Willard, P. A.; Hoover, M. D.; Hubbs, A. F. Efficacy of a Technique for Exposing the Mouse Lung to Particles Aspirated from the Pharynx. *J. Toxicol. Environ. Health A* **2003**, *66*, 1441–1452.
48. Folch, J.; Lees, M.; Sloane Stanley, G. H. A Simple Method for the Isolation and Purification of Total Lipides from Animal Tissues. *J. Biol. Chem.* **1957**, *226*, 497–509.